

Cite this: *Phys. Chem. Chem. Phys.*, 2011, **13**, 9978–9981

www.rsc.org/pccp

Nanoscale chemical imaging of segregated lipid domains using tip-enhanced Raman spectroscopy†

Lothar Opilik,^a Thomas Bauer,^{‡b} Thomas Schmid,^{‡a} Johannes Stadler^a and Renato Zenobi^{*a}

Received 9th December 2010, Accepted 9th March 2011

DOI: 10.1039/c0cp02832k

Lipid domains in supported lipid layers serve as a popular model to gain insight into the processes associated with the compartmentalization of biological membranes into so-called lipid rafts. In this paper, we present reproducible tip-enhanced Raman spectra originating from a very small number of molecules in a lipid monolayer on a gold surface, probed by the apex of a nanometer-sized silver tip. For the first time, we show large (128 × 128 pixels), high-resolution (< 50 nm) tip-enhanced Raman images of binary lipid mixtures with full spectral information at each pixel.

According to the lipid raft concept, phase segregation into lipid domains is involved in processes like protein sorting and signaling in biological membranes.¹ Direct visualization of these small and highly dynamic domains in the complex environment of a cellular membrane is a very challenging task. Phase segregated giant vesicles^{2,3} as well as supported lipid mono- and bilayers⁴ with known chemical composition have therefore often been used as model systems. The size of the segregated phase domains ranges from tens of nanometers to several microns.

Fluorescence microscopy is a common technique for the visualization of coexisting domains in model membranes as well as cellular membranes.^{2,3,5} However, epifluorescence and confocal fluorescence microscopy are diffraction limited and cannot be used to visualize domains with a size below 200 nm using light in the visible spectral range. The most common technique to visualize these very small lipid domains in supported membranes is atomic force microscopy (AFM).^{6–8} This is mainly achieved by measuring the difference in height and friction force of coexisting phase domains in mixed mono- and bilayers. In contrast to spectroscopic methods, AFM yields no or very limited chemical information. For multi-component mixtures with complex morphology, the purely topographic information is not sufficient to understand the distribution of all constituents within membrane leaflets.

Different attempts have been made to combine the high spatial resolution of scanning probe microscopy (SPM) with the rich chemical information provided by spectroscopy. One such technique called aperture scanning near-field optical microscopy (SNOM) has already been used successfully to perform fluorescence microscopy on model⁴ and biological membranes⁹ with a typical lateral resolution of 50–100 nm. The main idea of the technique is to excite fluorophores with a confined light source at the end of a small-aperture optical probe, which can be scanned across the sample surface.

However, in order to gain insight into the compartmentalization of biological membranes based on fluorescence microscopy, fluorescent probes with known partitioning preference for one of the coexisting phases are required. The phase preference for a given fluorescent probe can be different for different lipid systems and therefore has to be evaluated for each model system. Moreover, some of these fluorescent lipid analogues are known to perturb the phase behavior of lipid mixtures.¹⁰ This also limits the application of other fluorescence-based high-resolution imaging techniques, such as STED, STORM and PALM.¹¹

Methods based on Raman spectroscopy give the possibility for label-free chemical identification of coexisting lipid phases in membrane model systems under physiological conditions. The main challenge when working with spontaneous Raman scattering is the intrinsic weakness of the Raman scattering process. To counteract this, methods for enhanced Raman scattering have been developed. It has, for example, been shown that coherent anti-Stokes Raman scattering (CARS) is sensitive enough to acquire lipid spectra from single mono- and bilayers^{12,13} to allow for quantitative imaging on mixed lipid bilayers with a lateral resolution of 250 nm.¹⁴ Another method resulting in an enhanced Raman scattering intensity is tip-enhanced Raman spectroscopy (TERS).¹⁵ It is an apertureless near-field technique, where a metallic or metallized SPM tip is used to confine and enhance an electromagnetic field in close proximity to the sample surface. The main advantages compared to CARS are the better lateral resolution (15–40 nm)^{16,17} and the fact that TERS allows for the collection of a full spectrum at each point, whereas CARS is restricted to one selected Raman band. Tip-enhanced Raman spectra in the fingerprint region (<1800 cm⁻¹) collected on a single spot on a mixed supported lipid bilayer have been recently shown.¹⁸

^a Department of Chemistry and Applied Biosciences, ETH Zurich, CH-8093 Zurich, Switzerland. E-mail: zenobi@org.chem.ethz.ch; Fax: +41 44 6321292; Tel: +41 44 6324377

^b Department of Materials, ETH Zurich, CH-8093 Zurich, Switzerland

† Electronic supplementary information (ESI) available: Experimental and data processing details, and additional figures. See DOI: 10.1039/c0cp02832k

‡ These authors contributed equally to the work.

In this paper, we demonstrate that it is possible to collect reproducible and strongly enhanced tip-enhanced Raman spectra from lipid monolayers in the gap between a silver tip and a flat gold surface using top-illumination and STM feedback control.¹⁶ This configuration can be employed to image the lateral distribution of the individual components in a monolayer composed of a binary mixture of phospholipids with chemical selectivity.

The experiments were performed using a combined AFM/STM/Raman microscope (NT-MDT, Russia, NTEGRA Spectra Upright) described in more detail elsewhere.¹⁶ A HeNe laser with a wavelength of 632.8 nm was used as excitation source. AFM was done using nose-type silicon tips (ATEC-NC from Nanosensors) in semi-contact mode. As STM tips electrochemically etched silver wires (diameter of 0.25 μm , 99.99% purity, Aldrich) were used.¹⁶

Template-stripped (TS) gold surfaces were used as substrates. The preparation procedure is described elsewhere.¹⁹ After mechanical cleavage, the substrates were air-plasma treated for one minute to render the Au surface hydrophilic. Subsequently, they were directly immersed in Milli-Q water. 1,2-Dioleoyl-*sn*-glycero-3-phosphocholine (DOPC), 1,2-dipalmitoyl-*sn*-glycero-3-phosphocholine (DPPC) and 1,2-dipalmitoyl(d62)-*sn*-glycero-3-phosphocholine (d62-DPPC) were purchased from Avanti Polar Lipids (Alabaster, AL) and used without further purification. Binary lipid mixtures were prepared with a molar ratio of 1 : 1. Monolayers were prepared on a Langmuir–Blodgett (LB) trough (Minitrough, KSV, Finland) placed on an anti-vibration table in a dust-reduced environment, using Milli-Q water as the liquid phase. For every experiment, the deposition of the compounds was as follows: a 1 mg mL⁻¹ CHCl₃ solution was spread onto the water and the solvent was allowed to evaporate for 10 min. The total amount of the used CHCl₃ solution was 25 μL for DPPC, DOPC and d62-DPPC, whereas 20 μL were used for the DPPC/DOPC and the d62-DPPC/DOPC mixtures. The compression rate was set to 2 mm min⁻¹. The surface pressure was measured with a Wilhelmy balance with a precision of 0.01 mN m⁻¹. Structural annealing was performed by two compression/expansion cycles between the final pressure (10 mN m⁻¹ for DPPC, DOPC, the DPPC/DOPC mixture and 20 mN m⁻¹ for the d62-DPPC/DOPC mixture) and 2 mN m⁻¹. Subsequently, the monolayers were transferred onto TS gold and mica *via* vertical Langmuir–Blodgett technique with 2 mm min⁻¹. All monolayer transfers were done at room temperature. DPPC (saturated fatty acid chains) and DOPC (unsaturated fatty acid chains) are immiscible at room temperature and at a surface pressure of 10 mN m⁻¹, DPPC is predominantly present in condensed phase domains protruding from a surrounding fluid phase that consists mainly of DOPC.²⁰

A representative AFM topography image of a mixed LB monolayer of DPPC and DOPC deposited on freshly cleaved mica is shown in Fig. 1a. The step height of approx. 1 nm at the domain edges (see the corresponding line cross-section) is consistent with the literature value.²⁰ The array of parallel stripe domains is most likely formed by shear force-induced alignment and coalescence during vertical transfer or substrate-mediated condensation.^{21,22} Fig. 1b shows the AFM topography of the same mixed monolayer transferred onto TS gold. In this case,

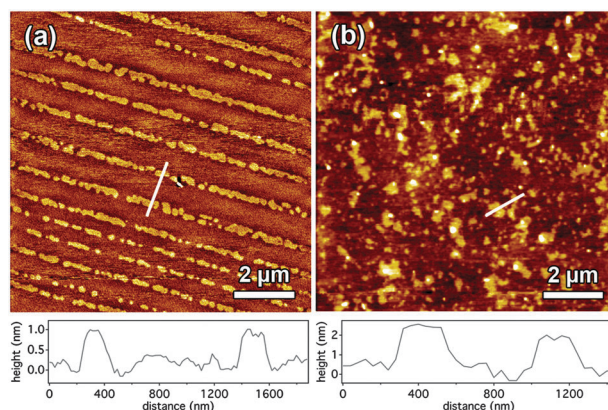


Fig. 1 Semi-contact mode AFM topography images of a DPPC/DOPC mixed monolayer (molar ratio of 1 : 1) transferred to mica (a) and TS gold (b) by Langmuir–Blodgett technique at room temperature. Cross-sections along the indicated lines are shown below the images.

the domains are not ordered, presumably due to the different surface properties compared to mica. The increased step height seen in the line cross-section could be the result of a higher stiffness difference between the two coexisting lipid phases resulting in a higher difference in penetration of the AFM tip at high oscillation damping (50%) in semi-contact mode. Such artifacts in AFM semi-contact imaging of lipid layers resulting in apparent topography differences that are affected by mechanical properties of the lipid agglomerate and tapping force are already described in the literature.²³ Monolayer

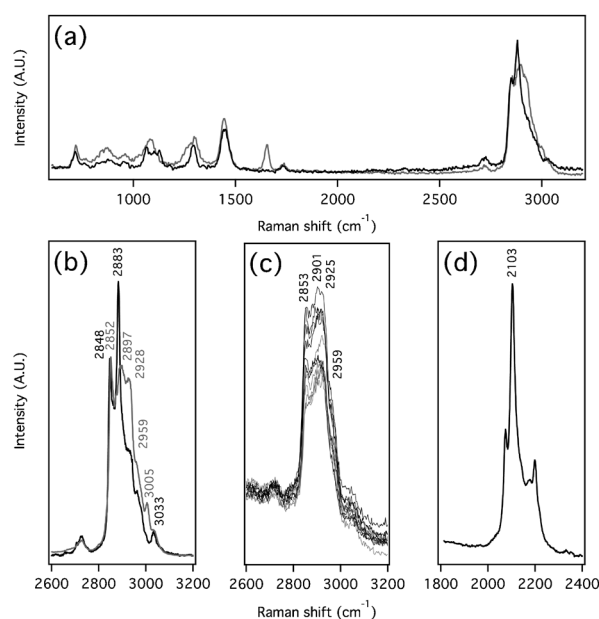


Fig. 2 Raman spectra of DPPC (black) and DOPC (gray) powder over the full spectral range (a) and in the C–H stretching region (b). TER spectra (c) from 6 different tip positions on a pure DPPC (black) and DOPC (gray) monolayer show similarities with the reference Raman spectra. The bulk Raman spectrum of d62-DPPC in the C–D stretching region (d) shows a similar peak at lower wavenumbers. The spectral resolution of 4.4 cm⁻¹ in (a) and (c) and of 0.8 cm⁻¹ in (b) and (d) depends on the used spectrometer grating.

deposition was only possible after air–plasma treatment of the TS gold surface, which shows the importance of removing residual organic impurities to ensure sufficient hydrophilicity of the gold surface.

Raman spectra of lipids show a strong band close to 2900 cm^{-1} corresponding to the methylene stretching vibrations of the long acyl chains which can be used as a marker band to visualize their distribution within a biological system.²⁴ Fig. 2 shows Raman spectra of DPPC and DOPC powders over the full spectral range (a) and in the C–H stretching region (b). The C–H stretching region of DPPC is dominated by the symmetric and antisymmetric methylene stretching vibrations at 2848 cm^{-1} and 2883 cm^{-1} . The lower chain order of the DOPC molecules results in reduced signal intensity for the antisymmetric methylene stretching vibration (in direct comparison to the symmetric stretching vibration) and a shift of both peaks to higher wavenumbers.¹² The weak signal at 3005 cm^{-1} that is only observed in the spectrum of DOPC is assigned to the vinylic C–H vibrations. At a slightly higher Raman shift of 3033 cm^{-1} both spectra exhibit a band associated with the antisymmetric methyl stretch of the choline head group.²⁵

Fig. 2c shows tip-enhanced Raman spectra in the C–H stretching region collected at random tip positions on a pure DPPC and DOPC monolayer, respectively, deposited on TS gold. An acquisition time of $40 \times 0.5\text{ s}$ was used for each spectrum, with an illumination laser power of $650\text{ }\mu\text{W}$ reaching the sample. The Raman bands at 2853 cm^{-1} , 2901 cm^{-1} , 2925 cm^{-1} and 2959 cm^{-1} are consistent with the bands from reference spectra. However, it is not possible to distinguish the two lipid compounds based on their C–H stretching vibrations.

To improve spectroscopic contrast, DPPC was substituted by d62-DPPC with fully deuterated lipid chains, which results in a C–D Raman band at 2100 cm^{-1} (see Fig. 2d), which is separated from any other lipid band. Due to the high degree of deuteration, the phase transition temperature of d62-DPPC is lowered by $5\text{ }^\circ\text{C}$ compared to the protiated DPPC.²⁶ This alteration was taken into account by increasing the surface pressure in the LB experiment (see above and the ESI†).

Fig. 3a and b show the AFM phase images of the mixed LB monolayer of d62-DPPC and DOPC on mica and TS gold, respectively. The morphology of the d62-DPPC domains looks rather similar on the two substrates. Fig. 3c shows a 26×64 pixel STM-TERS overview scan of a $6 \times 15\text{ }\mu\text{m}$ sample region (corresponding to a step size of 234 nm) and Fig. 3d reveals a 128×128 pixel STM-TERS scan on the marked area with an edge length of $6\text{ }\mu\text{m}$ (step size of 47 nm). The brightness of each pixel reflects the ratio of the C–D and the C–H band intensity for a collection time of 0.5 s per point and a laser power of $150\text{ }\mu\text{W}$ (overview scan) and $300\text{ }\mu\text{W}$ (high-resolution scan), respectively. The bright pixels in both images therefore exhibit a predominance of d62-DPPC molecules directly underneath the tip. The observed concentration of these d62-DPPC dominated spots in micrometre-sized areas is in agreement with the known phase separation behavior of the binary system (see above). The high-resolution scan in the highlighted region of the overview scan shows a similarly shaped domain,

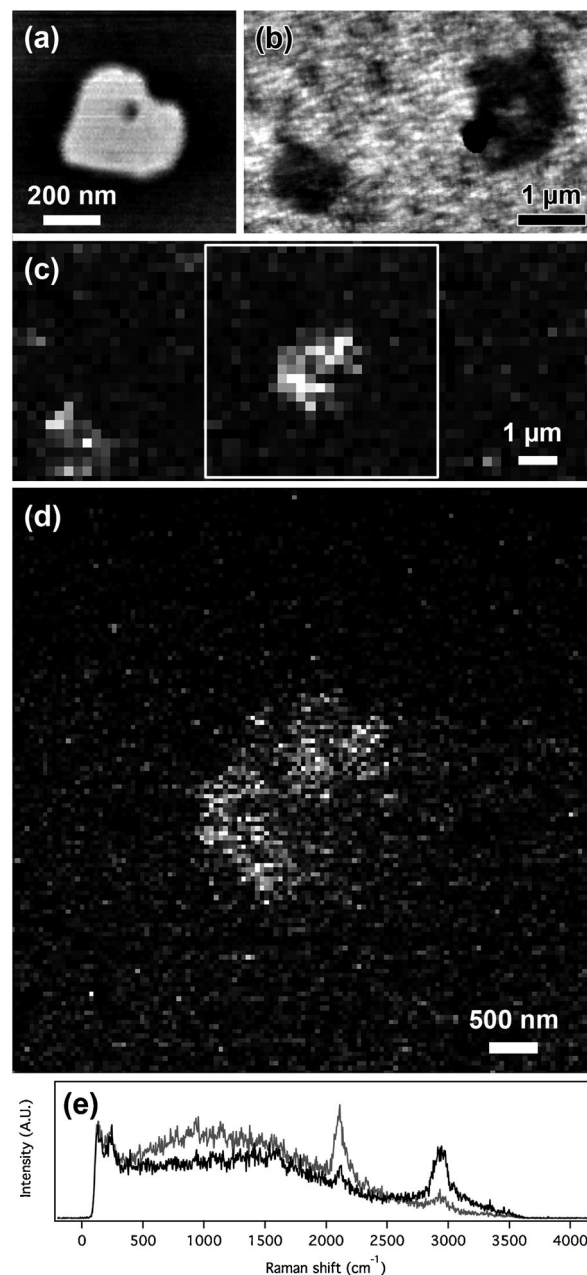


Fig. 3 Semi-contact mode AFM phase images of a d62-DPPC/DOPC mixed monolayer (molar ratio of 1 : 1) transferred to mica (a) and TS gold (b) by Langmuir–Blodgett technique at room temperature. STM-TERS images with 26×64 pixels (c) and 128×128 pixels (d) from two consecutive raster scans in the same region (the area of (d) is indicated in (c) with a white box) on a mixed monolayer on TS gold reveal a micron-sized structure. The brightness of each pixel indicates the intensity ratio of the Raman bands at 2100 cm^{-1} (C–D stretching vibrations) and 2900 cm^{-1} (C–H stretching vibrations). The Raman spectra from a dark (black) and a bright (gray) pixel of the high-resolution scan (e) illustrate the relative intensity change of the two mentioned Raman bands.

clearly demonstrating the reproducibility of the technique as well as its non-destructive fashion. Fig. 3e shows selected spectra from a bright pixel (gray) and from a dark pixel (black) extracted from the 128×128 pixel full spectrum scan illustrating the clear difference in band intensity of the two

marker bands. Both marker bands are observed in almost every spectrum of the TERS map with a sufficient signal-to-noise ratio: in 95% of the cases the peak values of the bands are larger than six times the standard deviation of the observed noise level. By plotting the intensity ratio of the two Raman bands instead of individual signal intensities, local and temporal fluctuations in the TERS enhancement are eliminated. It can therefore be assumed that pixel-to-pixel intensity variations reflect true concentration differences of the two lipid compounds in the corresponding sample volume.

Previous experiments with the same experimental setup¹⁶ show that the used step size of 47 nm is well above the actual lateral resolution (≤ 15 nm), which is given by the tip geometry and the gap size. From the surface pressure–area isotherm of the d62-DPPC/DOPC mixed monolayer at room temperature (see the ESI†) it has been derived that at a transfer pressure of 20 mN m^{-1} , each molecule occupies an area of approx. 71 \AA^2 on average. When we consider a lateral resolution of 15 nm we can estimate an average of 250 molecules contributing to each Raman spectrum. No reliable estimation for the achieved signal enhancement was possible, because no Raman bands could be obtained from a single lipid monolayer in the absence of the enhancing silver tip.

Conclusions

In this work, we used TER spectra in the C–H stretching region for the first time to demonstrate that it is possible to obtain reproducible Raman bands from a very small number of lipid molecules. Moreover, the lipid distribution in a mixed supported lipid monolayer was directly measured with high lateral resolution resulting in the first full-spectral images on phase separated lipid domains. By plotting the ratio of the marker bands, we significantly improve image contrast by reducing variations in signal enhancement during TERS raster scanning. This evaluation method could be potentially applied to any other TERS mapping experiment. Future investigations could focus on TERS imaging using AFM feedback control, which would significantly widen the scope of possible lipid model systems because non-conducting substrates and thicker layers could be used. Scans with a step size of 15 nm or less could be carried out to confirm the lateral resolution limit of the method. Furthermore, we target similar experiments under physiological conditions supported by previous work from our group demonstrating the feasibility of AFM-TERS experiments in aqueous environments.²⁷

Acknowledgements

The authors thank Jia Pei from the Laboratory for Surface Science and Technology at the ETH Zurich for air–plasma treatment of the gold substrates and the ETH for funding this work *via* an Independent Investigators' Research Award (grant no. ETH-09 10-1).

References

- 1 K. Simons and E. Ikonen, *Nature*, 1997, **387**, 569.
- 2 J. Korlach, P. Schwille, W. W. Webb and G. W. Feigensohn, *Proc. Natl. Acad. Sci. U. S. A.*, 1999, **96**, 8461.
- 3 S. L. Veatch and S. L. Keller, *Biophys. J.*, 2003, **85**, 3074.
- 4 L. J. Johnston, *Langmuir*, 2007, **23**, 5886.
- 5 K. Gaus, E. Gratton, E. P. W. Kable, A. S. Jones, I. Gelissen, L. Kritharides and W. Jessup, *Proc. Natl. Acad. Sci. U. S. A.*, 2003, **100**, 15554.
- 6 Y. F. Dufrière, W. R. Barger, J.-B. D. Green and G. U. Lee, *Langmuir*, 1997, **13**, 4779.
- 7 F. Tokumasu, A. J. Jin, G. W. Feigensohn and J. A. Dvorak, *Biophys. J.*, 2003, **84**, 2609.
- 8 M.-C. Giocondi, D. Yamamoto, E. Lesniewska, P.-E. Milhiet, T. Ando and C. Le Grimmellec, *Biochim. Biophys. Acta, Biomembr.*, 2010, **1798**, 703.
- 9 T. S. van Zanten, J. Gómez, C. Manzo, A. Cambi, J. Buceta, R. Reigada and M. F. García-Parajo, *Proc. Natl. Acad. Sci. U. S. A.*, 2010, **107**, 15437.
- 10 S. L. Veatch, S. S. W. Leung, R. E. W. Hancock and J. L. Thewalt, *J. Phys. Chem. B*, 2007, **111**, 502.
- 11 S. W. Hell, *Science*, 2007, **316**, 1153.
- 12 G. W. H. Wurpel, J. M. Schins and M. Müller, *J. Phys. Chem. B*, 2004, **108**, 3400.
- 13 E. O. Potma and X. S. Xie, *ChemPhysChem*, 2005, **6**, 77.
- 14 L. Li, H. Wang and J.-X. Cheng, *Biophys. J.*, 2005, **89**, 3480.
- 15 B.-S. Yeo, J. Stadler, T. Schmid, R. Zenobi and W. Zhang, *Chem. Phys. Lett.*, 2009, **472**, 1.
- 16 J. Stadler, T. Schmid and R. Zenobi, *Nano Lett.*, 2010, **10**, 4514.
- 17 N. Anderson, A. Hartschuh and L. Novotny, *Nano Lett.*, 2007, **7**, 577.
- 18 R. Böhme, M. Richter, D. Cialla, P. Rösch, V. Deckert and J. Popp, *J. Raman Spectrosc.*, 2009, **40**, 1452.
- 19 E. A. Weiss, G. K. Kaufman, J. K. Kriebel, Z. Li, R. Schalek and G. M. Whitesides, *Langmuir*, 2007, **23**, 9686.
- 20 O. Coban, J. Popov, M. Burger, D. Vobornik and L. J. Johnston, *Biophys. J.*, 2007, **92**, 2842.
- 21 P. Moraille and A. Badia, *Langmuir*, 2002, **18**, 4414.
- 22 X. Chen, N. Lu, H. Zhang, M. Hirtz, L. Wu, H. Fuchs and L. Chi, *J. Phys. Chem. B*, 2006, **110**, 8039.
- 23 P. Moraille and A. Badia, *Angew. Chem., Int. Ed.*, 2002, **41**, 4303.
- 24 C. W. Freudiger, W. Min, B. G. Saar, S. Lu, G. R. Holtom, C. He, J. C. Tsai, J. X. Kang and X. S. Xie, *Science*, 2008, **322**, 1857.
- 25 F. Lhert, D. Blaudez, C. Heywang and J.-M. Turllet, *Langmuir*, 2002, **18**, 512.
- 26 D. D. Baldyga and R. A. Dluhy, *Chem. Phys. Lipids*, 1998, **96**, 81.
- 27 T. Schmid, B.-S. Yeo, G. Leong, J. Stadler and R. Zenobi, *J. Raman Spectrosc.*, 2009, **40**, 1392.